Yttrium manganese oxide phase stability and selectivity using lithium carbonate assisted metathesis reactions

Paul K. Todd, Antoinette M.M. Smith, and James R. Neilson*

Colorado State University, Department of Chemistry, Fort Collins, Colorado 80523-1872, United States

E-mail: james.neilson@colostate.edu

Abstract

In solid-state chemistry, stable phases are often missed if their synthesis is impractical, such as when decomposition or a polymorphic transition occurs at relative low temperature. In the preparation of complex oxides, reaction temperatures commonly exceed 1000 °C with little to no control of the reaction pathway. Thus, a prerequisite for exploring the synthesis of complex oxides is to identify reactions with intermediates that are kinetically competent at low temperatures, as provided by assisted metathesis reactions. Here, we study the assisted metathesis reaction: $Mn_2O_3 + 2.2\,YCl_3 \cdot 6\,H_2O + 3\,Li_2CO_3 \longrightarrow 2\,YMnO_3 + 5.8\,LiCl + 0.2\,LiYCl_4 + 3\,CO_2$ using *in situ* synchrotron X-ray diffraction. By changing the atmosphere, oxygen vs. inert gas, the reaction product changes from the over-oxidized perovskite $YMnO_{3+\delta}$ to the hexagonal $YMnO_3$ polymorph at the reaction temperature of 850 °C, respectively. Analysis of the reaction pathways reveals two parallel reaction pathways in forming $YMnO_3$ phases: (1) the slow reaction of metal oxides in a LiCl flux ($Y_2O_3 + Mn_2O_3 \xrightarrow{6LiCl} 2\,YMnO_3$) and (2) the fast reaction from ternary intermediates ($YOCl + LiMnO_2 \longrightarrow LiCl + YMnO_3$) . Control reactions reveal that both proposed pathways in isolation result in product formation, but the

direct preparation of ternary intermediates ($YOCl + LiMnO_2 \longrightarrow LiCl + YMnO_3$) occurs at lower temperatures (500 °C), shorter times (< 24 h), and forms nominally-stoichiometric orthorhombic $YMnO_3$. These ternary intermediates react at a faster rate than the slow stepwise oxygenation of yttrium chloride to Y_2O_3 ($YCl_3 \longrightarrow YOCl \longrightarrow Y_3O_4Cl \longrightarrow Y_2O_3$), which is relatively inert. These results support a kinetically controlled reaction pathway to form $YMnO_3$ phases in assisted metathesis reactions with phase selectivity achievable through changes to reaction atmosphere.

Introduction

Current computational studies are able to predict millions of new functional materials,[1] but they are unable to successfully predict the synthetic pathways by which they proceed.[2] While computational studies have begun working towards modeling the "synthesizability" of new inorganic materials,[3,4] the focus remains on describing the thermodynamic range of the products' stability in relation to a thermodynamic energy ground-state.[5–7] While understanding the relative thermodynamic energetic position of a desired material is useful in accessing the probability of synthesizing a material,[8] current computational tools cannot predict synthetic variables as they relate to reaction kinetics, precursor competence, and non-equilibrium phase behavior.[4] Also, there is a growing list of stable compounds previously thought to not exist or be unstable, owing to their decomposition under traditional synthesis conditions (e.g., $MgCr_2S_4$).[9] Thus, more diagnostic studies are required that focus on characterizing these transient steps in material synthesis so that kinetic factors can be applied to these valuable data-driven endeavors.

In situ X-ray diffraction provides a powerful characterization tool for analyzing these kinetic factors in solid-state inorganic synthesis.[10,11] Temperature-dependent diffraction experiments have been used in characterizing kinetic control in solids,[12] thin films,[13] polymorph metastability,[14] battery kinetics,[15] hydrothermal crystal growth,[16] and the discovery of new materials in flux-mediated synthesis.[17] As a system for these diagnostic studies, metathesis reactions provide diverse compositional control in the synthesis of oxides, sulfides, and nitrides.[18] By tuning the reaction compo-

sition, energetics can be modulated from rapid, exothermic propagation events[19] to reactions that require continual heating.[20–22] These kinetically slower, non-propagating pathways provide opportunities for kinetic control at low-temperatures[23,24] and have been shown to synthesize metastable products.[12,14]

Previously, "assisted" metathesis reactions were shown to exhibit selective polymorph formation in the yttrium manganese oxide family of materials through changes in precursor reactivity.[25] Changing the alkali cation in the reaction between Mn_2O_3, YCl_3, and A_2CO_3 (where A = Li, Na, K) creates different kinetic pathways that result in three distinct yttrium manganese oxide products: orthorhombic $YMnO_{3+\delta}$, $Y_2Mn_2O_7$, and hexagonal $YMnO_3$. Each reaction involving an alkali cation represents a different set of synthesis conditions and nuances that lead to polymorph selectivity in this system. This contribution elaborates on lithium carbonate assisted-metathesis reactions.

Using lithium carbonate, the over-oxidized o-$YMnO_{3+\delta}$ appears to be the thermodynamically-stable product at reaction temperatures below 850 °C using oxidizing conditions and long reaction times (7 d):

$$\begin{aligned} &Mn_2O_3 + 2.2\,YCl_3\cdot 6\,H_2O + 3\,Li_2CO_3 \xrightarrow{O_2} \\ &2\,YMnO_{3+\delta} + 5.8\,LiCl + 0.2\,LiYCl_4(g) \\ &+ 3\,CO_2(g) + 12.4\,H_2O(g)\cdot \end{aligned} \tag{1}$$

At temperatures above 850 °C, or under inert conditions, the hexagonal $YMnO_3$ product dominates over long reaction times (7 d). While the over-oxidized perovskite phase is accessible via assisted metathesis, the stoichiometric o-$YMnO_3$ phase remains inaccessible using assisted metathesis at any temperature. Stoichiometric o-$YMnO_3$ has been labeled as metastable via citrate decomposition routes,[26,27] kinetic trapping,[28,29] and hydrothermal reactions,[30,31] but the kinetic factors that dictate why o-$YMnO_3$ forms over h-$YMnO_3$ are unclear.

The assisted metathesis reactions using lithium carbonate form the o-$YMnO_{3+\delta}$ polymorph,

but understanding the kinetic factors in selecting between this over-oxidized orthorhombic phase and the hexagonal polymorph may provide clarity on how to access stoichiometric o-$YMnO_3$. The assisted metathesis reactions are undoubtedly affected by oxygen fugacity, which suggests the over-oxidized o-$YMnO_{3+\delta}$ may be stabilized solely through inclusions of Mn(IV) defects and cation vacancies which have been observed in other rare-earth manganese oxides ($LnMnO_3$ where Ln = La, Pr, Nd).[32–35] While both orthorhombic phases form in the same space group (*Pbnm*), the over-oxidized phase exhibits a slightly contracted unit cell volume and exhibits different magnetic properties.[25]

Using *in situ* synchrotron X-ray diffraction, temperature-dependent assisted-metathesis reactions (Eq. 1) are examined under different reaction environments (O_2 vs. noble gas). Identification of the crystalline transient intermediates leads to the identification of two reaction pathways that explain the observation of o-$YMnO_3$ formation: The formation and subsequent reaction of (i) ternary intermediates YOCl and $LiMnO_2$ and/or (ii) binary oxides in a lithium chloride flux. In testing these hypotheses using *ex situ* control reactions, we identify both pathways as competent intermediates but discover that the ternary metathesis reaction between yttrium oxychloride and lithium manganese oxide is much more kinetically competent (i.e., it is faster). Using the discovered "ternary" metathesis between YOCl and $LiMnO_2$, stoichiometric o-$YMnO_3$ is shown to be synthetically accessible at low-temperatures (500 °C).

Methods

All reagents were prepared, stored, and weighed in an argon-filled glovebox with O_2 and H_2O levels $\leq$ 0.1ppm. Manganese(III) oxide (Sigma Aldrich 99%) was purified by heating Mn_2O_3 in an alumina boat at 1 °C/min to 700 °C for 16 h in air and quenched into the glovebox; purity was verified by powder X-ray diffraction (PXRD). $YCl_3 \cdot 6H_2O$ (Alfa Aesar 99.9%), lithium carbonate (Sigma Aldrich 99.9%), lithium iodide (Alfa Aesar 99.5%), and lithium choride (Alfa Aesar 99.5%), were purchased and stored under argon. All gases (O_2, Ar, He) were purchased through

Airgas at the Ultra High Purity grade (99.999%). $NaMnO_2$ ($C2/m$) was prepared by mixing manganese (III) oxide and sodium carbonate (Sigma Aldrich 99.9%) in a 1:1 molar ratio, grinding for 15 minutes in an agate mortar and pestle, and pelleting using $\sim$1 tn of force. The pellet was placed upon a sacrificial layer of powder in an alumina crucible and heated in a muffle furnace at 1 °C/min to 700 °C for 10 h. The reaction was subsequently quenched into the antechamber of the glovebox and stored under argon. $LiMnO_2$ ($C2/m$) was prepared through a solid-state ion exchange from $NaMnO_2$ and LiI. Sodium manganese oxide was mixed with three molar equivalents of lithium iodide, placed in an alumina crucible, which was sealed in a quartz ampule under vacuum ($>$ 10 mTorr). The reaction was heated at 1 °C/min to 460 °C for 4 h and cooled at 1 °C/min to room temperature. The product was washed with deionized water, filtered, and dried at 80 °C for 6 h. YOCl was prepared by heating $YCl_3 \cdot 6H_2O$ in an alumina boat to 350 °C at 10 °C/min for 4 h in air. The YOCl product formed is the $P4/nmn$ PbClF structure-type. All prepared reactants were confirmed using laboratory PXRD. Preparations for *ex situ* assisted metathesis reactions have been described in detail previously.[25] Oxygen partial pressure was controlled using mass flow controllers to achieve a 1:100 dilution of oxygen in argon ($pO_2 \sim 10^{-2}$ atm), flowing argon ($pO_2 \sim 10^{-6}$ atm), and flowing oxygen ($pO_2 \sim$0.8 atm).

For temperature-dependent *in situ* assisted metathesis reactions that produce carbon dioxide as a by-product, open-ended quartz capillary (1.1 mm OD) were packed in a glove-bag under argon using glass wool as a plug. Synchrotron X-ray diffraction experiments were performed at beamline 17-BM-B (λ = 0.2415) at the Advanced Photon Source at Argonne National Laboratory using a Perkin Elmer plate detector at a distance of 700 mm. All capillaries were loaded into a flow-cell apparatus equipped with resistive heating elements and heated at 10 °C/min.[36] Gas flow (O_2, He) was supplied at APS and controlled through mass flow controllers at a rate of 0.2 cc/min. Assisted-metathesis reactions were heated to a maximum temperature of 850 °C while the sample continuously rocked at $\pm$ 5° about the length of the capillary. Diffraction patterns were collected every two seconds and summed every 20 seconds for powder averaging. Plate detector images were integrated using GSAS-II and calibrated using a LaB_6 standard. Laboratory PXRD data were

collected on a Bruker D8 Discover diffractometer using Cu Kα radiation and a Lynxeye XE-T position-sensitive detector.

All Rietveld refinements were performed using TOPAS v6. Due to the number and positional overlap of intermediates during the sequential refinements, all thermal displacement parameters were fixed at 5^2 and the full-width-half-max was fixed at 178 nm to better account for changes in peak intensity during the reaction. In order to compare the relative fractions of phases determined from Rietveld calculations, a weighted scale factor is defined as: $Q_p = S_p \cdot V_p \cdot M_p$ where Q_p = weighted scale factor of phase p, S_p = Scale factor calculated from Rietveld for phase p, V_p is the volume of the unit cell for phase p, and M_p is the atomic mass of the unit cell for phase p. It should be noted that we omit the Brindley coefficient for microabsorption correction in our calculation of weighted scale factor due to the inability to successfully refine our particle sizes for individual phases. Amorphous material and product lost as vapor are not accounted for in the sequential refinement. We reference all phases by their stoichiometric formula; however, the actual chemical formula may be distinct from the written formula as XRD data alone cannot typically resolve non-stoichiometric compounds.

Results

In situ synchrotron X-ray diffraction experiments were performed to study reaction progress as a function of temperature (25 °C $\geq$ T $\leq$ 850 °C; 10 °C/min) and environment (O_2 vs. Ar/He). Figure 1(a) shows the integrated SXRD patterns from the assisted metathesis reaction (Eq. 1) under flowing oxygen as a function of temperature. As precursors are heated, the reaction progress can be segmented into discrete reactive zones (I, II, III). To quantitatively visualize these reactive zones, sequential Rietveld refinements were performed over the range of diffraction patterns and the results are represented in Figure 1(b), where each horizontal sub-panel highlights a different cation (Y, Mn, Li) for clarity.

Reactive zone I describes the reaction of yttrium chloride with lithium carbonate (T_{rxn}=25-320

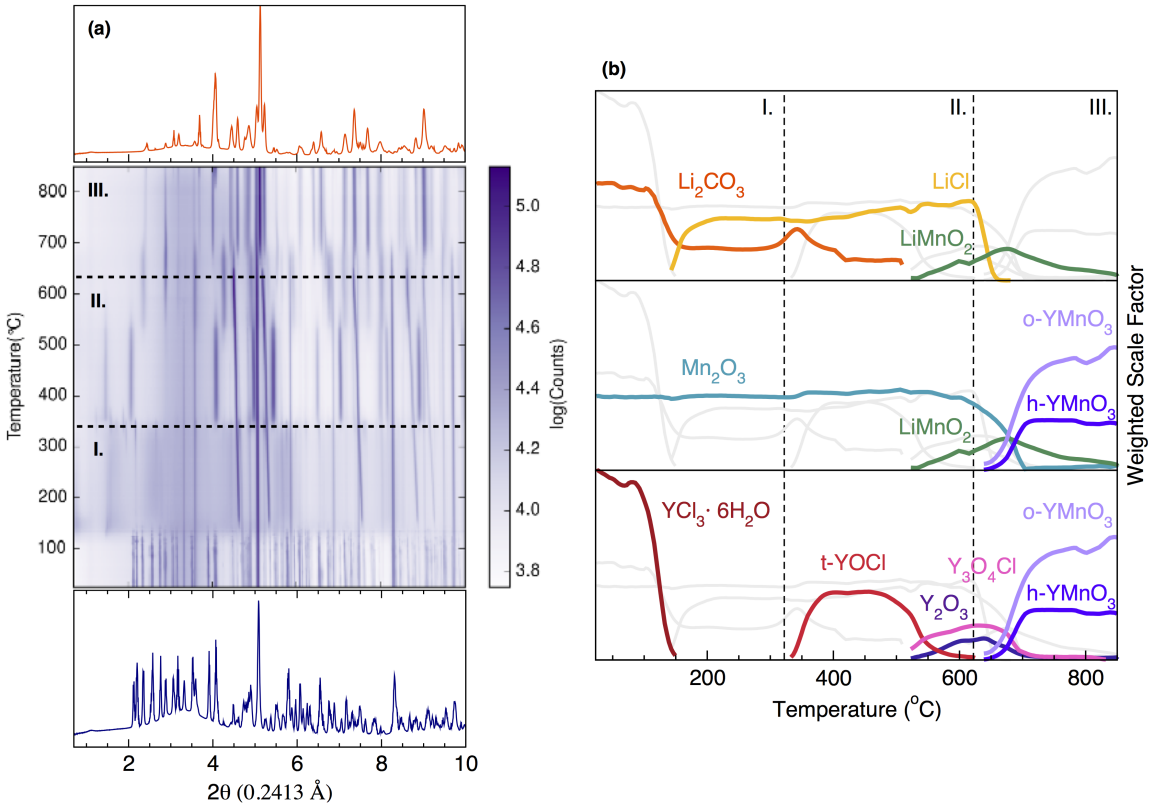

Figure 1: *In situ* PXRD results of the reaction: $Mn_2O_3 + 2.2\,YCl_3 \cdot 6H_2O + 3Li_2CO_3$ under flowing oxygen. (a) Powder diffraction patterns as a function of temperature (b) Weighted scale factor of each phase during the reaction pathway from Rietveld refinement as a function of temperature. Both (a) and (b) are separated into three reactive zones: I Reactivity of yttrium chloride and formation of YOCl; II Oxygenation of YOCl and formation of $LiMnO_2$; III Melting of LiCl and $YMnO_3$ formation. Each sub-panel in (b) is separated by cation for visualization purposes with the gray lines denoting phases with other cations.

°C). The first reaction in Zone I is the dehydration of $YCl_3 \cdot 6H_2O$ which occurs in the two-step process:

$$YCl_3 \cdot 6H_2O \longrightarrow YCl_3 \cdot H_2O + 5H_2O(g) \tag{2a}$$

$$YCl_3 \cdot H_2O \longrightarrow YCl_3 + H_2O(g) \tag{2b}$$

TGA-MS results (Figure 2) support the two-step dehydration of yttrium chloride which agrees with

previous studies on the decomposition of rare-earth chloride hydrates in air.[37] Upon dehydration, the yttrium chloride reacts with two moles of lithium carbonate according to the following reaction at T_{rxn}=155-320 °C:

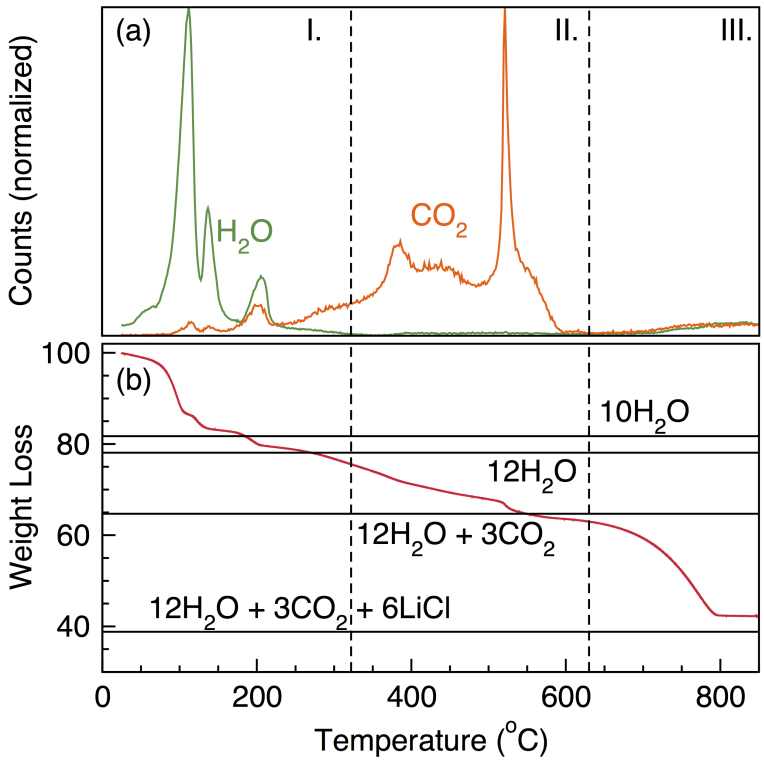

Figure 2: (a) mass spectrometry and (b) thermogravimetric analysis on the reaction: $Mn_2O_3 + 2\,YCl_3 \cdot 6\,H_2O + 3\,Li_2CO_3$. The reaction was heated at 10 °C/min to 850 °C with reaction zones I, II, and III presented for comparison to Figure 1. The theoretical mass loss from the reaction are shown as solid black lines in (b). Release of H_2O and CO_2 vapor during the reaction matches the reactivity observed in the *in situ* SXRD data.

$$2\,YCl_3 + 2\,Li_2CO_3 \longrightarrow 2\,YOCl + 4\,LiCl + 2\,CO_2 \tag{3}$$

The formation of LiCl at 136 °C and decrease in Li_2CO_3 peak intensity over this temperature range is supported in Rietveld analysis (Figure 1) and mass loss with an increase in CO_2 ion count (Figure 2). Interestingly, there is a discontinuity in crystalline yttrium containing phases (Figure 1) after the loss of intensity of yttrium chloride hexahydrate. Visual inspection of the SXRD data

also shows an increase in intensity near the background that correspond to poorly resolved YOCl ($R\bar{3}m$) reflections. These reflections grow (155 -322 °C) before this YOCl phase undergoes a phase transition to the $P4/mnm$ structure at 322 °C. During Zone I, the manganese(III) oxide remains unchanged.

Reaction Zone II (322-630 °C) describes the behavior of ternary intermediates along the reaction pathway. During this temperature range, lithium chloride continues to increase in intensity and lithium carbonate decreases slowly in intensity (Figure 1). TGA-MS (Figure 2) supports the reactivity of lithium carbonate as both mass loss and the ion count of CO_2 steadily increases over this range. An increase in lithium carbonate intensity is observed at 350 °C in Figure 1 due to the overlapping peak positions with $P4/mnm$ YOCl, which grows in rapidly at this temperature. The behavior of the yttrium-containing intermediates over this range is indicative of the conversion to Y_2O_3 under flowing oxygen; as $P4/mnm$ YOCl reacts, Y_3O_4Cl and Y_2O_3 emerge while LiCl continues to grow.

At 515 °C, Mn_2O_3 reacts with the remaining Li_2CO_3 according to the reaction in Equation 4:

$$Mn_2O_3 + Li_2CO_3 \longrightarrow 2\,LiMnO_2 + CO_2 \tag{4}$$

TGA-MS (Figure 2) shows a sharp increase in the CO_2 signal at this temperature, supporting the reaction with Mn_2O_3. Crystalline $LiMnO_2$ ($C2/m$, Figure 1) begins to grow at 515 °C, while the Mn_2O_3 begins to lose intensity.

Reactive Zone III (620-650 °C) begins with the melting of lithium chloride at 620 °C and ends with the formation of $YMnO_3$ products. During this zone, the Mn_2O_3 loses intensity rapidly as LiCl melts. Concomitantly, the intensity of $LiMnO_2$ grows over this range. At 630 °C, the nucleation and growth of both h-$YMnO_3$ and o-$YMnO_{3+\delta}$ occurs. Above this temperature, all remaining ternary intermediates react while both $YMnO_3$ phases grow. TGA-MS (Figure 2) shows a large mass loss above this temperature that is associated with the volatilization of lithium chloride,

which has been observed previously in assisted metathesis reactions involving lithium carbonate.[25] Unfortunately, lithium chloride also corrodes the quartz capillary at this temperature, as evidenced by the increase in crystalline SiO_2 at $\sim 4^\circ$ 2θ (Figure 1). Thus, *in situ* isothermal studies at such elevated reaction temperatures are not viable as the capillary disintegrates over time. The formation of both hexagonal and orthorhombic $YMnO_3$ polymorphs occurs simultaneously at 630 °C. As temperature increases, the amount of o-$YMnO_{3+\delta}$ increases at a faster rate than the hexagonal polymorph.

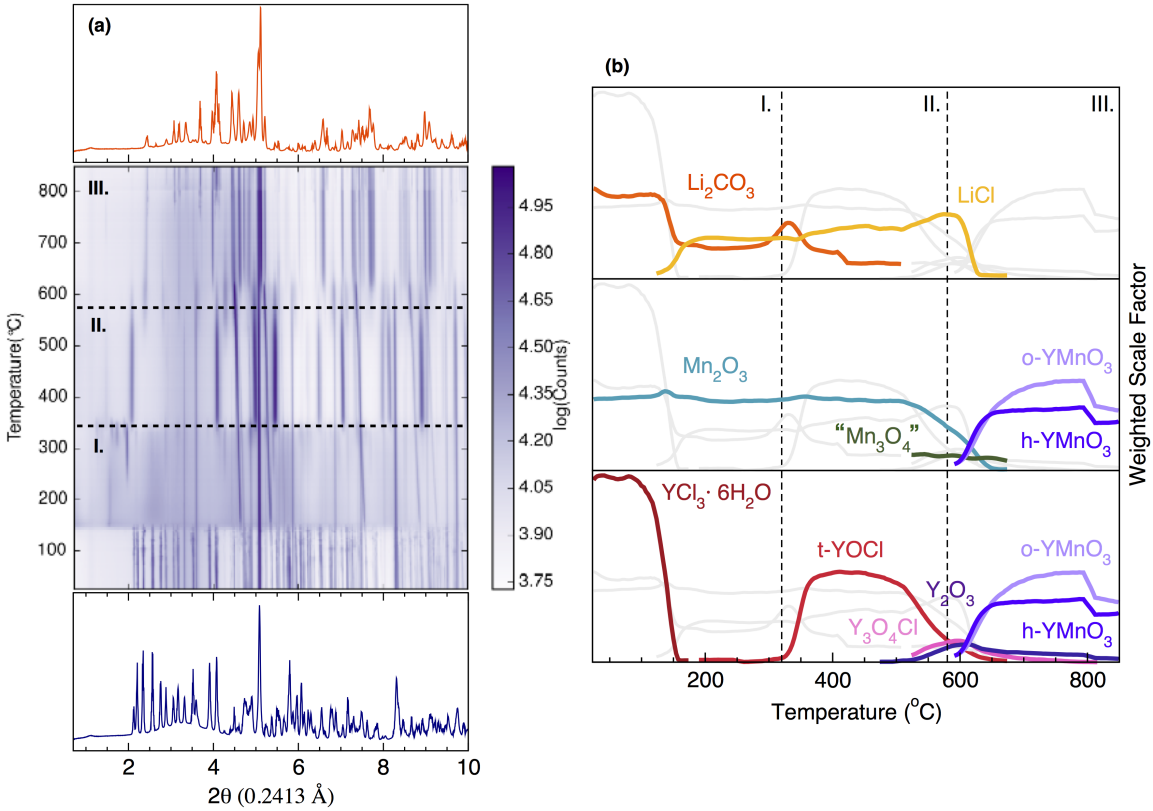

Figure 3: *In situ* PXRD results of the reaction: $Mn_2O_3 + 2.2\,YCl_3 \cdot 6H_2O + 3\,Li_2CO_3$ under flowing helium. (a) Powder diffraction patterns as a function of temperature (b) Weighted scale factor of each phase during the reaction pathway from Rietveld refinement as a function of temperature. Both (a) and (b) are separated into three reactive zones: I Reactivity of yttrium chloride and formation of YOCl; II Oxidation of YOCl and formation of $LiMnO_2$; III Melting of LiCl and $YMnO_3$ formation. Each sub-panel in (b) is separated by cation for visualization purposes with the gray lines denoting phases with other cations. Quotation marks denote that Mn_3O_4 is poorly resolved from $Li_2Mn_2O_4$ in our refinement.

To test the role of reaction atmosphere on the observed products, the assisted metathesis re-

action in Equation 1 was performed under flowing helium while monitoring the reaction progress with *in situ* SXRD. Figure 3 shows the integrated diffraction patterns as a function of temperature along with the calculated scale of relevant phases from Rietveld analysis during the reaction. Reactive zones I, II, and III (Figure 3) follow the same general trends as Figure 1 with the exception of two major differences. First, there is no distinguishable formation of the ternary intermediate $LiMnO_2$ during the reaction under helium. During Zone II, the only crystalline intermediate that forms when Mn_2O_3 reacts is the spinel Mn_3O_4. It should be noted that this phase is poorly resolved in the diffraction data and possesses the same space group as the tetragonal spinel "$Li_2Mn_2O_4$" ($I4_1/amd$) with comparable unit cell parameters. The second difference is observed upon the formation and growth of $YMnO_3$ phases in Zone III Under flowing helium, where the formation of $YMnO_3$ phases occurs at 580 °C as compared to 630 °C under flowing oxygen. Also, both hexagonal and orthorhombic polymorphs seem to grow at comparable rates during heating. This contrasts with the reaction performed in O_2 (g) (Figure 1), where the orthorhombic polymorph grows at a much faster rate as compared to the hexagonal polymorph. A drop in intensity of all phases is observed above 800 °C in Figure 3 due to degradation of the capillary.

Ex situ reactions show that the atmosphere changes which phase of $YMnO_3$ dominates after extended duration reactions. Under flowing oxygen, the orthorhombic phase selectively forms after 4 hours (Fig. 4(a)). Reactions performed at 850 °C under flowing argon show both h-$YMnO_3$ and o-$YMnO_3$ form upon heating while longer reactions form h-$YMnO_3$ as the observed product. Analysis of the calculated unit cell volume (Fig. 4(b)) using different environments supports the oxidation to o-$YMnO_{3+\delta}$ when performing the reaction under flowing oxygen.

Additionally, control reactions were performed at various temperatures and oxygen partial pressures to understand how oxygen fugacity affects phase formation. The relative amounts of each $YMnO_3$ product are displayed in Figure 5 as individual pie charts. It is likely that these reactions do not fully equilibrate after 24 h; as such, we assume the majority product to be most stable under the experimental conditions. At high temperatures, regardless of oxygen partial pressure, the hexagonal polymorph dominates. At high oxygen partial pressures the o-$YMnO_3$ phase forms

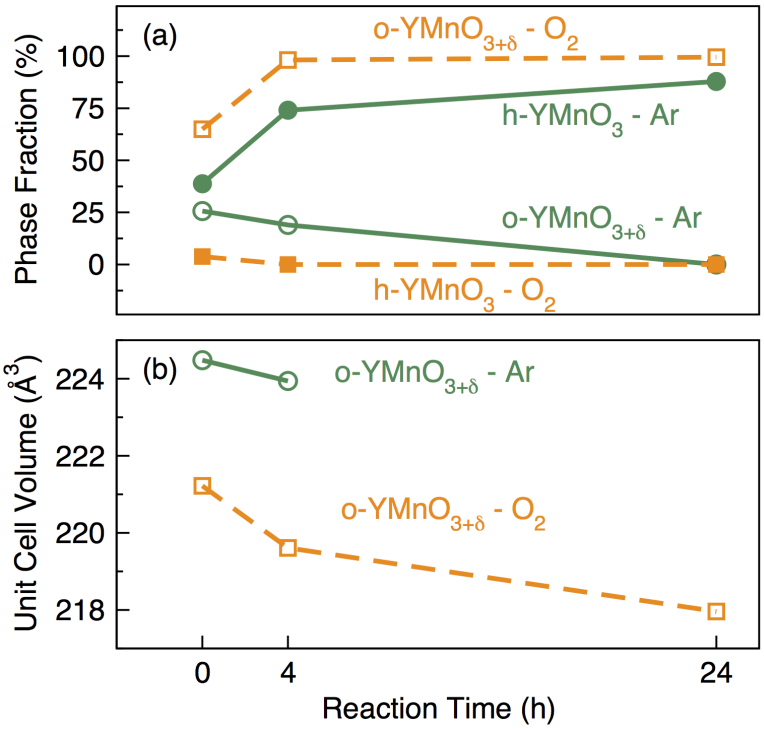

Figure 4: (a) $YMnO_3$ products calculated from *ex situ* assisted metathesis reactions at 850 °C (Eq 1.) under flowing argon (green) versus oxygen (orange) at various reaction times. Open symbols represent the calculated phase fraction of o-$YMnO_{3+\delta}$ while solid symbols show the phase fraction of h-$YMnO_3$. (b) Calculated volumes of o-$YMnO_{3+\delta}$ products from the reactions in (a). The reactions performed under flowing oxygen show a decrease in reaction volume as a function of time.

over the temperature range of 550-850 °C. At temperatures below 700 °C and $pO_2 < 1$atm, mixed products of h-$YMnO_3$ and stoichiometric o-$YMnO_3$ appear. At temperatures below 550 °C no $YMnO_3$ products are observed.

Analysis of the crystalline intermediates along the reaction pathway leads to the construction of two primary hypotheses that lead to $YMnO_3$ formation:

$$YOCl + LiMnO_2 \longrightarrow LiCl + YMnO_3 \tag{5}$$

$$Y_2O_3 + Mn_2O_3 \xrightarrow{6LiCl} 2\,YMnO_3 \tag{6}$$

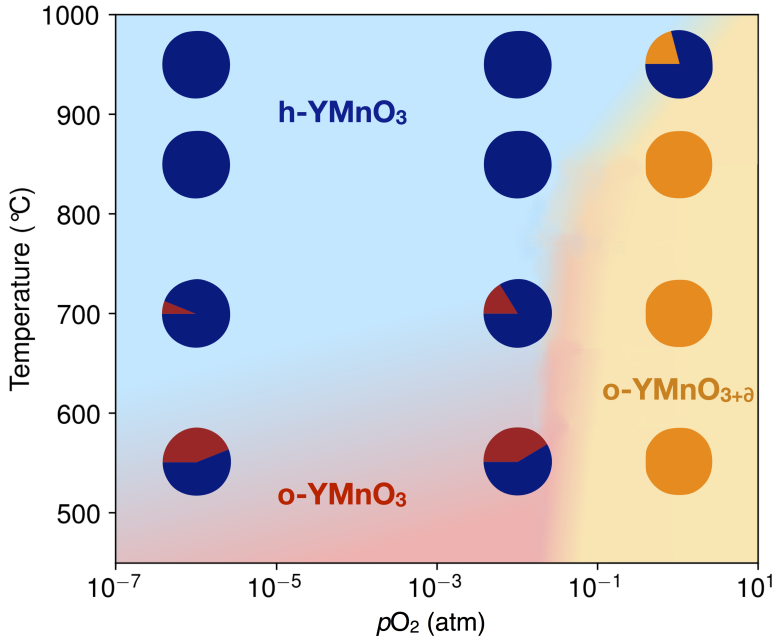

Figure 5: (a) $YMnO_3$ products calculated from *ex situ* assisted metathesis reactions at various temperatures and oxygen partial pressures (Eq 1.). Each pie chart denotes the relative molar phase fraction of each $YMnO_3$ phase as calculated from Rietveld refinements after 24 h reactions: navy = h-$YMnO_3$, red = o-$YMnO_3$, and orange = o-$YMnO_{3+\delta}$. Shaded regions illustrate the qualitative change in phase formation under the presented conditions. At high temperatures, h-$YMnO_3$ dominates. At high oxygen partial pressures and temperatures below 850 °C the over-oxidized o-$YMnO_{3+\delta}$ forms selectively. At temperatures below 750 °C and lower oxygen partial pressures, a mixture of h-$YMnO_3$ and o-$YMnO_3$ are observed.

In order to test the viability of each hypothesized reaction, *ex situ* control reactions were performed and the diffraction patterns of the products are shown in Figure 6 & 7. The reaction between ternary intermediates (Eq. 5, 500 °C, 24 h, *in vacuo*) shows the formation of o-$YMnO_3$ as the main product (Fig 6(a)) while the reaction from the oxides in a lithium chloride flux (Eq. 6) remains predominately binary oxides (Fig. 7(a)). If the temperature for the flux reaction is increased to 600 °C for 24 h, o-$YMnO_3$ partially forms (Fig. 7(b)), while at 850 °C h-$YMnO_3$ is the major product after 24 h (Fig. 7(c)). Compared to the reaction shown in Equation 5, the reaction from the oxides requires higher temperatures and longer times than the reaction from ternary intermediates, even in a LiCl flux. In the assisted metathesis reactions formation of the orthorhombic product depends on an oxygen-rich reaction environment, but the control reactions shown in Figure 6 both are performed *in vacuo*. Unit cell volumes calculated from Rietveld refinements confirmed that the

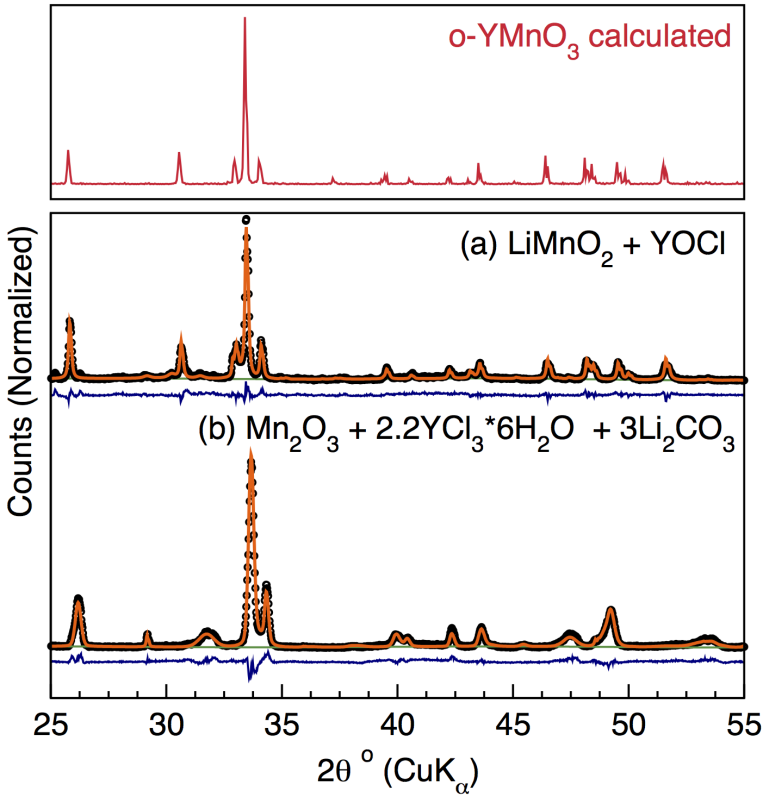

Figure 6: Comparison of *ex situ* reactions (a) $LiMnO_2 + YOCl$, 500 °C, 24 h, < 10 mTorr; and (b) $Mn_2O_3 + 2.2\,YCl_3 \cdot 6\,H_2O + 3\,Li_2CO_3$, 850 °C, 24 h, Flowing O_2. Both reactions were heated at 10 °C/min. The calculated X-ray diffraction pattern is provided for o-$YMnO_3$ from the ICSD. The product in (a) matches the stoichiometric o-$YMnO_3$ while the pattern in (b) shows differences in peak position and shape for the o-$YMnO_{3+\delta}$ phase.

unit cell volume of the o-$YMnO_3$ formed in Equation 5 (225.39 ^{3}) matches that of single crystal o-$YMnO_3$ (225.56^3);[30] over-oxidized $YMnO_{3.11}$ has a unit cell volume contraction (219.97^3).[25] Comparison of the PXRD data of $YMnO_{3.11}$ from assisted metathesis reactions at 850 °C for 24 h in flowing oxygen is displayed in Figure 6(b) to show the change in peak position and anisotropic peak broadening of the over-oxidized phase. The calculated orthorhombic $YMnO_3$ matches the o-$YMnO_3$ product from ternary metathesis (Fig. 6(a)). Therefore, we conclude that the orthorhombic phase formed in Figure 6(a) is stoichiometric and not the over-oxidized polymorph (Fig. 6(b)).

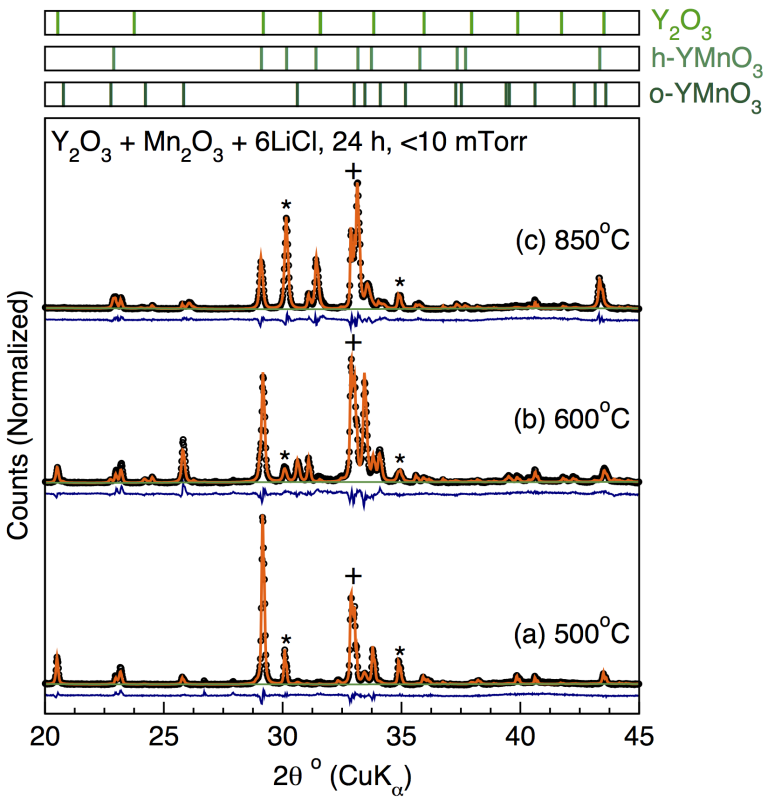

Figure 7: Comparison of *ex situ* reactions from the reaction: $Y_2O_3 + Mn_2O_3 \xrightarrow{6LiCl}$ at (a) 550 °C (b) 600 °C (c) 850 °C. All reactions were heated at 10 °C/min to the reaction temperatrue for 24 h under vacuum in a sealed quartz ampule. Reported structures from ICSD are denoted as tick marks. Main reflections for $LiCl \cdot H_2O$: + and LiCl: $*$ are present but not identified using tick marks.

Discussion

The collective results from these *in situ* SXRD experiments using assisted metathesis reveal a kinetically-controlled reaction pathway that proceeds through transient intermediates. Analysis of these crystalline intermediates and their reaction temperature regimes illustrates the competence of assisted metathesis precursors to overcome diffusion limitations in the formation of complex oxides. Previous studies on the kinetics of complex oxide formation are inherently limited to studying diffusion, whether that be in the bulk,[38] thin-films,[39] or hydrothermally.[40] The sluggish reaction kinetics in oxides can be attributed to the slow rate of diffusivity of larger cations within the oxygen sub-lattice, as seen in the synthesis of ternary metal titanates ($BaTiO_3$, $SrTiO_3$) and

rare-earth chromium oxides ($LaCrO_3$, $YCrO_3$).[41–43] These observations are supported in previous studies on $YMnO_3$ formation, where reactions from the binary oxides ($Y_2O_3 + Mn_2O_3$) are limited by the refractory nature of yttrium oxide. Even at elevated temperatures and times (900 °C, 96 h) the reaction products include unreacted Y_2O_3 and yttrium-poor YMn_2O_5.[25] Assisted metathesis reactions overcome this diffusion barrier by starting with labile precursors (e.g., YCl_3) that react at lower temperatures.

The presented results illustrate that the choice of reaction environment in the assisted metathesis reactions changes the thermodynamic stability of the product. Previous studies have shown that oxygen fugacity can affect polymorph stability in TiO_2 polymorphs by favoring defect states in the anatase polymorph at high oxygen fugacities.[44] We have demonstrated that high oxygen fugacity (Fig. 5) in assisted metathesis reactions results in the formation of o-$YMnO_{3+\delta}$ at high oxygen partial pressures. At partial pressures below 1 atm, the hexagonal polymorph dominates at all temperatures, although at 550 °C, nominally o-$YMnO_3$ forms as a minority product. These data suggest that o-$YMnO_3$ may be accessible at low temperatures and oxygen partial pressures. Unfortunately, assisted metathesis reactions do not form any yttrium manganese oxide products below 550 °C as Mn_2O_3 is not reactive at this temperature. Thus, if o-$YMnO_3$ is the desired product, a different reaction pathway is needed that competently forms $YMnO_3$ products below 550 °C.

Analysis of the reaction intermediates from Figures 1 and 3 provide two hypothetical reactions (Eq. 5 & 6) for the formation of $YMnO_3$ products. Equation 5 proposes a metathesis reaction from ternary intermediates that are observed along the reaction pathway. While YOCl forms and reacts comparably under flowing oxygen and argon, the formation of $LiMnO_2$ is only apparent in the reaction pathway under flowing oxygen. When Mn_2O_3 begins to react under flowing helium in Figure 3, Mn_3O_4 appears as the only manganese containing intermediate. The mixed-valent Mn_3O_4 spinel ($I4_1/amd$) is poorly resolved in the diffraction data over the temperature range observed (580-680 °C) due to a large number of present phases that overlap in intensity. Interestingly, the nominally tetragonal spinel "$Li_2Mn_2O_4$" ($I4_1/amd$) also exists with similar lattice parameters as Mn_3O_4. Mn_3O_4 is used in the sequential refinement as the intermediate in Figure 3 as the

Rietveld calculations have improved statistics (Mn_3O_4 R_wp = 9.886, $Li_2Mn_2O_4$ R_wp = 10.356) during this temperature range. While Mn_3O_4 provides the best statistical fit to the data, we cannot rule out that $Li_2Mn_2O_4$ is not present in some amount at this temperature under flowing helium. Thus, we deduce that the ternary metathesis reaction in Equation 5 is a plausible pathway for the formation of $YMnO_3$, regardless of environment.

The reaction from binary oxides in a lithium chloride flux (Eq. 6) is derived from the two observations from the reaction pathways: (1) the eventual formation of Y_2O_3 from yttrium chloride precursors and (2) the observed T_{rxn} of Mn_2O_3 coinciding with the melting of LiCl. Alkali halide fluxes have been used previously to accelerate the synthesis of yttrium silicates[45] and are used extensively as fluxes in the growth of single crystal complex oxides.[46] Thus, if both binary oxides are present in a molten, reactive environment (LiCl T_m = 605 °C), the activation barrier of yttrium oxide diffusion can be lowered to form $YMnO_3$.

While each proposed hypothesis can explain the observed formation of $YMnO_3$, *ex situ* control reactions reveal that the rate at which each reaction proceeds differs. The reaction from the ternary intermediates (Eq. 5, Fig. 6(a)) proceeds at lower temperatures and shorter times than the reaction from the binary oxides using a lithium chloride flux (Eq. 6, Fig. 7(a)). Even at higher temperatures (Figure 7(b,c)), the reaction from the oxides is still incomplete after 24 h. The assisted metathesis reactions proceed to completion at reaction times as low as 4 h at 850 °C suggesting that the formation and reaction between ternary intermediates is kinetically-controlling the reaction pathway.

Analysis of these ternary reaction intermediates reveals why they are kinetically competent at lower temperatures. Both $P4/nmn$ YOCl and $C2/m$ $LiMnO_2$ adopt layered structures (Fig. 8) that facilitate and increase diffusion as compared to the structurally dense binary oxides which adopt the cubic $Ia\bar{3}$ structure (Fig. 8). The $C2/m$ $LiMnO_2$ adopts a disordered α-$NaFeO_2$-type structure with slight site mixing between the lithium and manganese. All yttrium containing intermediates ($R\bar{3}m$ YOCl, $P4/nmn$ YOCl, $Cmcm$ Y_3O_4Cl) form ordered layers of alternating oxygen and chlorine bilayers separated by yttrium. The YOCl begins forming at temperatures much lower than the formation of $LiMnO_2$, but the slow conversion to Y_2O_3 allows for these layered intermediates to

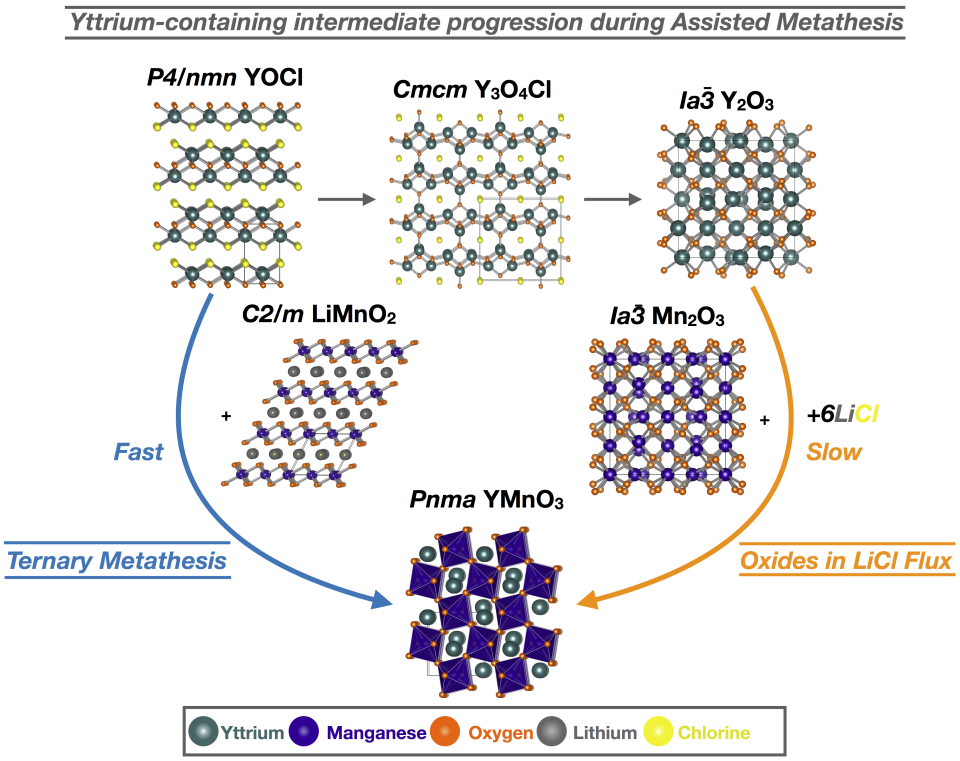

Figure 8: Comparison of the structures for the proposed intermediate reactions in Equations 5 & 6 as derived from characterization of the assisted metathesis reaction pathway. Yttrium-containing intermediates were derived from characterizing the the assisted metathesis reaction pathways (Fig. 1 & 3). From *ex situ* control reactions the ternary metathesis reaction ($YOCl + LiMnO_2$) is the kinetically controlling reaction pathway and, while still a competent reaction pathway, the reaction from binary oxides in a lithium chloride flux ($Y_2O_3 + Mn_2O_3 \xrightarrow{6LiCl}$) requires longer reaction times to arrive at the orthorhombic $YMnO_3$ product.

persist long enough to react to form $YMnO_3$. The structurally-dense $Ia\bar{3}$ Y_2O_3 does form during the reaction pathway but reacts upon the melting of LiCl. Therefore, the ternary metathesis reaction between $LiMnO_2$ and YOCl is the most competent pathway, but it is not the only reaction pathway possible during an assisted metathesis reaction.

Taken together, three unique reaction conditions enable competent low-temperature, selective syntheses of three different $YMnO_3$ phases (Table 1). The identification and development of ternary metathesis reactions has been previously shown using lithium manganese oxide and lanthanum oxychloride to form $LaMnO_3$ at 850 °C for 12 h.[21] By reducing the reaction temperature even further (850 °C to 500 °C), the ternary metathesis permits the formation of o-$YMnO_3$, which

Table 1: Conditions for selective synthesis of $YMnO_3$ phases

Phase	o-$YMnO_3$	o-$YMnO_{3+\delta}$	h-$YMnO_3$
Space Group	*Pbnm*	*Pbnm*	$P6_3cm$
Reaction Type	Ternary metathesis (Eq. 5)	Assisted Metathesis (Eq. 1) Ternary metathesis (Eq. 5) LiCl flux (Eq. 6)	Assisted Metathesis (Eq. 1) Ternary metathesis (Eq. 5) LiCl flux (Eq. 6)
Conditions	T <600 °C	T = 500 - 850 °C	T > 600 °C
Evironment	Vacuum, inert gas	O_2, air	Vacuum, inert gas

appears to be thermodynamically stable at these lower temperatures. Previous studies using hydrothermal[30,31] or citrate decomposition[26,27] pathways have resulted in the formation of o-$YMnO_3$ at similar temperatures, but the kinetic factors governing these reactions are more difficult to elucidate than the solid-state reactions studied here. The ternary metathesis reactions pose another system of kinetically competent reactions when considering new complex oxides: they are less complex than the three-component assisted metathesis systems and can be performed *in vacuo*, reducing the compositional complexity and improving phase selectivity. Future studies will aim to expand the compositional space of these reactions.

Conclusion

In situ SXRD has been used to characterize the reaction pathway in the assisted metathesis reaction: $Mn_2O_3 + 2.2\,YCl_3\cdot 6\,H_2O + 3\,Li_2CO_3 \longrightarrow 2\,YMnO_3 + 5.8\,LiCl + 0.2\,LiYCl_4(g) + 3\,CO_2 + 12.4\,H_2O$. It has been determined that the selectivity of reaction products is dependent on the reaction atmosphere. The over-oxidized perovskite o-$YMnO_{3+\delta}$ forms under flowing oxygen while the hexagonal $YMnO_3$ forms under inert conditions at 850 °C at long time points. While reaction atmosphere determines the product stability in assisted-metathesis, *in situ* analysis of the reaction progress identifies YOCl and $LiMnO_2$ as the intermediates that kinetically control formation of o-$YMnO_3$. Using these intermediates as precursors to perform ternary metathesis leads to the formation of nominally stoichiometric o-$YMnO_3$ at 500 °C. While molten LiCl may also enhance mass transport in the reaction, the ternary metathesis reaction yields products in a shorter amount

of time and at temperatures lower than the melting point of LiCl, as confirmed by *ex situ* control experiments.

Acknowledgement

This work was supported by the National Science Foundation (DMR-1653863). JRN acknowledges support from a Sloan Research Fellowship. We would like to acknowledge A. Martinolich and C. Rom for their assistance with SXRD experiments. We would also like to acknowledge the facilities at 17-BM-B at the Advanced Photon Source at Argonne National Laboratory and, in particular, the support of A. Yakovenko, W. Wu.

References

(1) Draxl, C.; Scheffler, M. NOMAD: The FAIR Concept for Big-Data-Driven Materials Science. **2018**, https://arxiv.org/abs/1805.05039.

(2) Soderholm, L.; Mitchell, J. F. Perspective: Toward synthesis by design: Exploring atomic correlations during inorganic materials synthesis. *APL Mater.* **2016**, *4*, 053212.

(3) Curtarolo, S.; Hart, G. L.; Nardelli, M. B.; Mingo, N.; Sanvito, S.; Levy, O. The high-throughput highway to computational materials design. *Nat. Mater.* **2013**, *12*, 191–201.

(4) Bartel, C. J.; Millican, S. L.; Deml, A. M.; Rumptz, J. R.; Tumas, W.; Weimer, A. W.; Lany, S.; Stevanović, V.; Musgrave, C. B.; Holder, A. M. Physical descriptor for the Gibbs energy of inorganic crystalline solids and temperature-dependent materials chemistry. *Nat. Commun.* **2018**, *9*, 4168.

(5) Sun, W.; Dacek, S. T.; Ong, S. P.; Hautier, G.; Jain, A.; Richards, W. D.; Gamst, A. C.; Persson, K. A.; Ceder, G. The thermodynamic scale of inorganic crystalline metastability. *Sci. Adv.* **2016**, *2*, e1600225–e1600225.

(6) Sun, W.; Holder, A.; Orvañanos, B.; Arca, E.; Zakutayev, A.; Lany, S.; Ceder, G. Thermodynamic Routes to Novel Metastable Nitrogen-Rich Nitrides. *Chem. Mater.* **2017**, *29*, 6936–6946.

(7) Zwijnenburg, M. A.; Bromley, S. T. Structural richness of ionic binary materials: An exploration of the energy landscape of magnesium oxide. *Phys. Rev. B - Condens. Matter Mater. Phys.* **2011**, *83*, 1–9.

(8) Aykol, M.; Hegde, V. I.; Hung, L.; Suram, S.; Herring, P.; Wolverton, C.; Hummelshøj, J. S. Network analysis of synthesizable materials discovery. *Nat. Commun.* **2019**, *10*, 1–20.

(9) Wustrow, A.; Key, B.; Phillips, P. J.; Sa, N.; Lipton, A. S.; Klie, R. F.; Vaughey, J. T.; Poeppelmeier, K. R. Synthesis and Characterization of $MgCr_2S_4$ Thiospinel as a Potential Magnesium Cathode. *Inorg. Chem.* **2018**, *57*, 8634–8638.

(10) Jiang, Z.; Ramanathan, A.; Shoemaker, D. P. In situ identification of kinetic factors that expedite inorganic crystal formation and discovery. *J. Mater. Chem. C* **2017**, *5*, 5709–5717.

(11) Martinolich, A. J.; Neilson, J. R. Toward Reaction-by-Design: Achieving Kinetic Control of Solid State Chemistry with Metathesis. *Chem. Mater.* **2017**, *29*, 479–489.

(12) Martinolich, A. J.; Kurzman, J. A.; Neilson, J. R. Circumventing Diffusion in Kinetically Controlled Solid-State Metathesis Reactions. *J. Am. Chem. Soc.* **2016**, *138*, 11031–11037.

(13) Koch, C.; Dankwort, T.; Hansen, A.-L.; Esters, M.; Häußler, D.; Volker, H.; von Hoegen, A.; Wuttig, M.; Johnson, D. C.; Bensch, W.; Kienle, L. Investigation of the phase change mechanism of $Ge_6Sn_2Sb_2Te_11$. *Acta Mater.* **2018**, *152*, 278–287.

(14) Martinolich, A. J.; Kurzman, J. A.; Neilson, J. R. Polymorph Selectivity of Superconducting $CuSe_2$ Through Kinetic Control of Solid-State Metathesis. *J. Am. Chem. Soc.* **2015**, *137*, 3827–3833.

(15) Liu, H.; Kazemiabnavi, S.; Grenier, A.; Vaughan, G.; Di Michiel, M.; Polzin, B. J.; Thornton, K.; Chapman, K. W.; Chupas, P. J. Quantifying Reaction and Rate Heterogeneity in Battery Electrodes in 3D through Operando X-ray Diffraction Computed Tomography. *ACS Appl. Mater. Interfaces* **2019**, *11*, 18386–18394.

(16) Birgisson, S.; Saha, D.; Iversen, B. B. Formation Mechanisms of Nanocrystalline MnO_2 Polymorphs under Hydrothermal Conditions. *Cryst. Growth Des.* **2018**, *18*, 827–838.

(17) Shoemaker, D. P.; Chung, D. Y.; Mitchell, J. F.; Bray, T. H.; Soderholm, L.; Chupas, P. J.; Kanatzidis, M. G. Understanding Fluxes as Media for Directed Synthesis: In Situ Local Structure of Molten Potassium Polysulfides. *J. Am. Chem. Soc.* **2012**, *134*, 9456–9463.

(18) Parkin, I. P.; Kafizas, A. *Comprehensive Inorganic Chemistry II (Second Edition: From Elements to Applications*; Elsevier Ltd., 2013; Vol. 2; pp 471–490.

(19) Bonneau, P. R.; Jarvis, R. F.; Kaner, R. B. Rapid solid-state synthesis of materials from molybdenum disulphide to refractories. *Nature* **1991**, *349*, 510–512.

(20) Gopalakrishnan, J.; Sivakumar, T.; Ramesha, K.; Thangadurai, V.; Subbanna, G. N. Transformations of Ruddlesden - Popper oxides to new layered perovskite oxides by metathesis reactions. *J. Am. Chem. Soc.* **2000**, *122*, 6237–6241.

(21) Mandal, T. K.; Gopalakrishnan, J. From rocksalt to perovskite: a metathesis route for the synthesis of perovskite oxides of current interest. *J. Mater. Chem.* **2004**, *14*, 1273.

(22) Parhi, P.; Ramanan, A.; Ray, A. R. Synthesis of nano-sized alkaline-earth hydroxyapatites through microwave assisted metathesis route. *Mater. Lett.* **2006**, *60*, 218–221.

(23) Martinolich, A. J.; Neilson, J. R. Pyrite Formation via Kinetic Intermediates through Low-Temperature Solid-State Metathesis. *J. Am. Chem. Soc.* **2014**, *136*, 15654–9.

(24) Martinolich, A. J.; Higgins, R. F.; Shores, M. P.; Neilson, J. R. Lewis Base Mediated Polymorph Selectivity of Pyrite $CuSe_2$ through Atom Transfer in Solid-State Metathesis. *Chem. Mater.* **2016**, *28*, 1854–1860.

(25) Todd, P. K.; Neilson, J. R. Selective Formation of Yttrium Manganese Oxides through Kinetically Competent Assisted Metathesis Reactions. *J. Am. Chem. Soc.* **2019**, *141*, 1191–1195.

(26) Muñoz, A.; Alonso, J. a.; Casais, M. T.; Martínez-Lope, M. J.; Martínez, J. L.; Fernández-Díaz, M. T. The magnetic structure of $YMnO_3$ perovskite revisited. *J. Phys. Condens. Matter* **2002**, *14*, 3285–3294.

(27) Gardner, J. S.; Gingras, M. J. P.; Greedan, J. E. Synthesis of Metastable Perovskite-type $YMnO_3$ and $HoMnO_3$. *Rev. Mod. Phys.* **2010**, *82*, 53–107.

(28) Iliev, M. N.; Abrashev, M. V.; Lee, H.-G.; Popov, V. N.; Sun, Y. Y.; Thomsen, C.; Meng, R. L.; Chu, C. W. Raman spectroscopy of orthorhombic perovskitelike $YMnO_3$ and $LaMnO_3$. *Phys. Rev. B* **1998**, *57*, 2872–2877.

(29) Fujinaka, H.; Kinomura, N.; Koizumi, M.; Miyamoto, Y.; Kume, S. Syntheses and physical properties of pyrochlore-type $A_2B_2O_7$ (A=Tl,Y; B=Cr,Mn). *Mater. Res. Bull.* **1979**, *14*, 1133–1137.

(30) Ishiwata, S.; Tokunaga, Y.; Taguchi, Y.; Tokura, Y. High-Pressure Hydrothermal Crystal Growth and Multiferroic Properties of a Perovskite $YMnO_3$. *J. Am. Chem. Soc.* **2011**, *133*, 13818–13820.

(31) Giaquinta, D. M.; zur Loye, H.-C. Structural Predictions in the ABO_3 Phase Diagram. *Chem. Mater.* **1994**, *6*, 365–372.

(32) Alonso, J. A.; Martínez-lope, M. J.; Casais, M. T.; Macmanus-driscoll, J. L.; de Silva, P. S. I. P. N.; Cohen, L. F.; Fernández-díaz, M. T. Non-stoichiometry, structural defects and

properties of $LaMnO_{3+\delta}$ with high δ values ($0.11 \leq \delta \leq 0.29$). *J. Mater. Chem.* **1997**, *7*, 2139–2144.

(33) Tofield, B. C.; Scott, W. R. Oxidative nonstoichiometry in perovskites, an experimental survey; the defect structure of an oxidized lanthanum manganite by powder neutron diffraction. *J. Solid State Chem.* **1974**, *10*, 183–194.

(34) Zuev, A. Y.; Tsvetkov, D. S. Oxygen nonstoichiometry, defect structure and defect-induced expansion of undoped perovskite $LaMnO_{3\pm\delta}$. *Solid State Ionics* **2010**, *181*, 557–563.

(35) Cherepanov, V.; Barkhatova, L.; Petrov, A.; Voronin, V. Oxygen Nonstoichiometry and Crystal and Defect Structure of $PrMnO_{3+y}$ and $NdMnO_{3+y}$. *J. Solid State Chem.* **1995**, *118*, 53–61.

(36) Chupas, P. J.; Chapman, K. W.; Kurtz, C.; Hanson, J. C.; Lee, P. L.; Grey, C. P. A versatile sample-environment cell for non-ambient X-ray scattering experiments. *J. Appl. Crystallogr.* **2008**, *41*, 822–824.

(37) Wendlandt, W. W. The thermal decomposition of yttrium, scandium, and some rare-earth chloride hydrates. *J. Inorg. Nucl. Chem.* **1957**, *5*, 118–122.

(38) Merkle, R.; Maier, J. How is oxygen incorporated into oxides? A comprehensive kinetic study of a simple solid-state reaction with SrTiO3 as a model material. *Angew. Chemie - Int. Ed.* **2008**, *47*, 3874–3894.

(39) Kotula, P. G.; Carter, C. B. Interfacial control of reaction kinetics in oxides. *Phys. Rev. Lett.* **1996**, *77*, 3367–3370.

(40) Eckert, J. O.; Hung-Houston, C. C.; Gersten, B. L.; Lencka, M. M.; Riman, R. E. Kinetics and Mechanisms of Hydrothermal Synthesis of Barium Titanate. *J. Am. Ceram. Soc.* **1996**, *79*, 2929–2939.

(41) Buscaglia, M. T.; Bassoli, M.; Buscaglia, V.; Vormberg, R. Solid-state synthesis of nanocrystalline $BaTiO_3$: Reaction kinetics and powder properties. *J. Am. Ceram. Soc.* **2008**, *91*, 2862–2869.

(42) Akashi, T. Solid-State Reaction Kinetics of $LaCrO_3$ from the Oxides and Determination of La^{3+} Diffusion Coefficient. *J. Electrochem. Soc.* **2006**, *145*, 2090.

(43) Kawamura, K.-i.; Saiki, A.; Maruyama, T.; Nagata, K. Diffusion Coefficient of Yttrium Ion in $YCrO_3$. *J. Solid State Sci. Technol.* **1995**, *142*, 3073–3077.

(44) Heald, E. F.; Weiss, C. W. Kinetics and mechanism of the anatase/rutile transformation, as catalyzed by ferric oxide and reducing conditions. *American Mineralogist* **1972**, *57*, 10–23.

(45) Leskela, M.; Jyrkas, K. Effect of Flux Materials on the Reaction of Y_2O_3 and SiO_2. *J. Am. Ceram. Soc.* **1987**, *70*, C160–C161.

(46) Boltersdorf, J.; King, N.; Maggard, P. A. Flux-mediated crystal growth of metal oxides: Synthetic tunability of particle morphologies, sizes, and surface features for photocatalysis research. *CrystEngComm* **2015**, *17*, 2225–2241.

Graphical TOC Entry

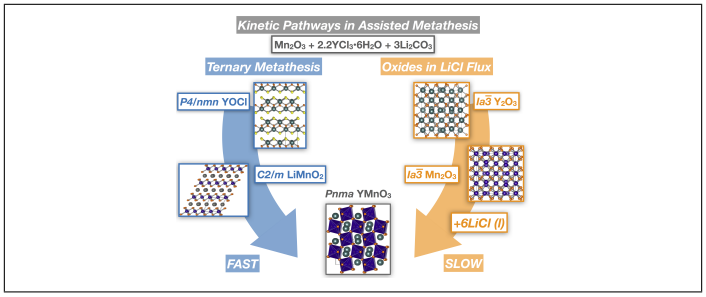

Lithium carbonate assisted metathesis reactions are shown to provide a low-temperature synthesis route to ternary $YMnO_3$ polymorphs when changing the reaction environment from flowing oxygen (orthorhombic $YMnO_{3+\delta}$) to flowing inert gas (hexagonal $YMnO_3$). *In situ* characterization of the reaction reaction reveals that the pathway is kinetically controlled by the formation of ternary intermediates: $YOCl + LiMnO_2$. When those are taken as precursors, stoichiometric o-$YMnO_3$ phase formation is possible at temperatures as low as 500 ℃.